ACS APPLIED MATERIALS & INTERFACES

Research Article

www.acsami.org

Novel α-Fe_2O_3/CdS Cornlike Nanorods with Enhanced Photocatalytic Performance

Ye Shi, Hanying Li,* Ling Wang, Wei Shen, and Hongzheng Chen*

State Key Laboratory of Silicon Materials, MOE Key Laboratory of Macromolecular Synthesis and Functionalization, & Department of Polymer Science and Engineering, Zhejiang University, Hangzhou 310027, P. R. China

ABSTRACT: Various semiconductors have been studied as photocatalysts for photocatalytic degradation of pollutants in aqueous solutions. As one of the promising visible-light-driven semiconductor photocatalysts, α-Fe_2O_3 has advantages of low cost and stability. However, its application is inhibited by the poor separation of photogenerated electron-hole pair. In this work, hybrid structures were prepared to improve the performance of α-Fe_2O_3. CdS nanoparticles were overgrown on the preformed single-crystalline α-Fe_2O_3 nanorods by a simple and mild one-step wet-chemical method, resulting in α-Fe_2O_3/CdS cornlike nanocomposites. X-ray diffraction (XRD), scanning electron microscopy (SEM), transmission electron microscopy (TEM), and Raman spectroscopy showed the α-Fe_2O_3/CdS core/shell heterostructure of the nanocomposite with high crystallinity. Furthermore, the cornlike nanocomposites exhibited superior photocatalytic performances under visible light irradiation over the pure α-Fe_2O_3 nanorods and CdS nanoparticles. The photocatalytic activity of the composites is superior to the previously-reported pure α-Fe_2O_3 nanomaterials, and the performance is comparable to both the commercial TiO_2 (P25) which is used under UV irradiation and the newly developed α-Fe_2O_3/SnO_2 photocatalyst under visible light irradiation. The enhanced performance is associated with the larger surface area of the cornlike structure, the crystalline nature of the materials and the synergy in light absorption and charge separation between α-Fe_2O_3 and CdS. As such, our α-Fe_2O_3/CdS cornlike nanocomposites may be promising to be used as visible-light-driven high-performance photocatalyst.

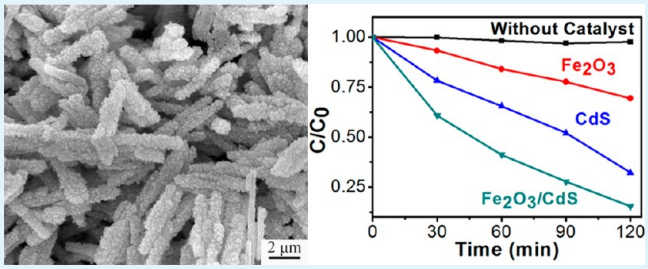

KEYWORDS: *α-Fe_2O_3, CdS, semiconductors, hybrid materials, visible-light-driven, photocatalyst*

INTRODUCTION

In recent years, one-dimensional (1D) nanostructures, such as nanorods,[1,2] nanobelts,[3] nanotubes,[4,5] and nanofibers[6] have attracted much interest because of their unique properties and diverse potential applications in catalysis,[7] photoelectric devices,[8] gas sensors[9] and magnetic materials.[10] Compared to single-component 1D nanomaterials, 1D heterostructures of semiconductors are of special interest because their optical, electronic, magnetic and chemical properties can be largely enhanced or modified.[11−14] Currently, much effort has been devoted to the synthesis of 1D heterostructures with different components.

Hematite (α-Fe_2O_3) is one of the most stable iron oxides with n-type semiconducting properties.[15] Because of its low cost, simple production, environmental friendliness, and excellent chemical stability, α-Fe_2O_3 has been intensively investigated in a variety of applications such as catalysts,[16] pigments,[17] water treatment,[18] magnetic materials,[19] sensors,[20] and lithium ion batteries.[21,22] With a low band gap of 2.2 eV, α-Fe_2O_3 absorbs most of the visible light, becoming a promising visible-light-driven photocatalyst. However, photo-induced electron-hole pairs in α-Fe_2O_3 are difficult to be separated, which inhibits its further application as an efficient photocatalyst.[11] Recently, many methods against its drawbacks have been reported. Among them, controlled synthesis of α-Fe_2O_3 with 1D morphology and synthesis of α-Fe_2O_3-based heterostructures have been proved to be two effective methods to improve the separation efficiency of photogenerated electron-hole pairs. Wang et al.[20] used a facile solution approach to synthesize highly stable porous α-Fe_2O_3 nanorods with a much higher response to ethanol as demonstrated by the gas-sensing measurement. Also, Peng et al.[11] synthesized Fe_2O_3/TiO_2 heterogeneous photocatalysts with different mass ratios by impregnation of Fe^{3+} on the surface of TiO_2. The heterojunction structure between Fe_2O_3 and TiO_2 improved the separation of photogenerated electrons and holes, and enhanced the photocatalytic activity. Similarly, Zhu et al.[23] obtained core−shell structured α-Fe_2O_3@SnO_2 nanocomposites and the degradation of the model molecule, Rhodamine B, showed that the nanocomposites had much higher photocatalytic activity than pure α-Fe_2O_3 or SnO_2.

CdS is another promising semiconductor with a direct band gap of 2.42 eV. However, CdS is susceptible to photocorrosion when used as photocatalyst in aqueous media.[14] One way to improve the stability of CdS is to couple it with another semiconductor with lower but closely lying conduction band

Received: June 25, 2012
Accepted: August 15, 2012
Published: August 15, 2012

dx.doi.org/10.1021/am3011516 | ACS Appl. Mater. Interfaces 2012, 4, 4800−4806

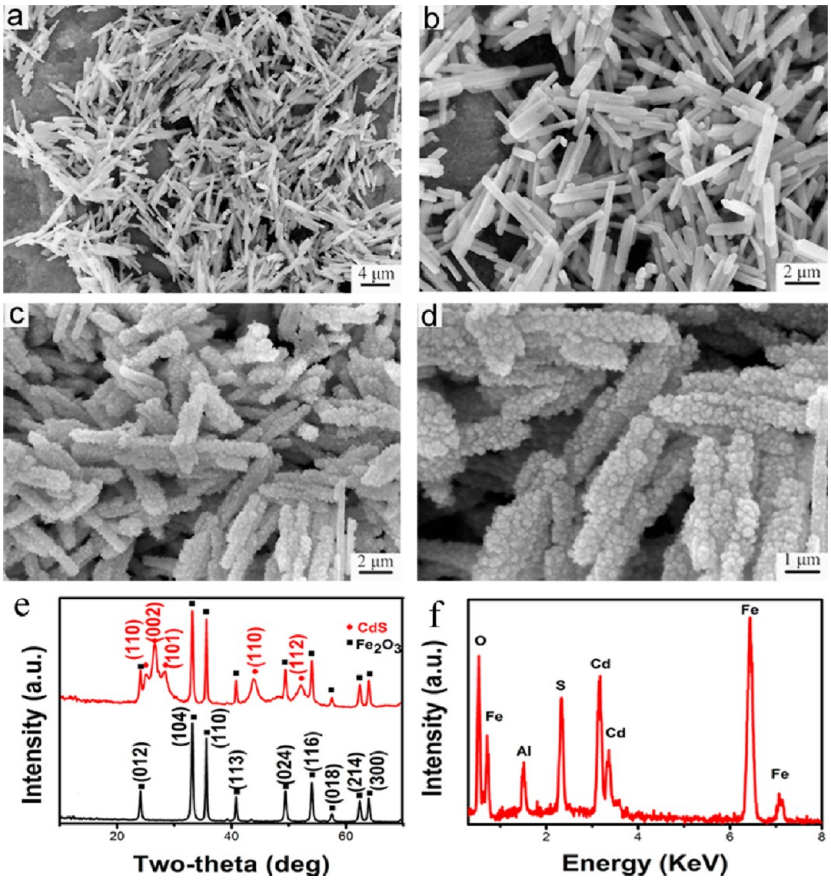

Figure 1. SEM images of (a, b) the pre-prepared α-Fe_2O_3 nanorods and (c, d) the α-Fe_2O_3/CdS nanocomposites; (e) XRD patterns of the pre-prepared α-Fe_2O_3 nanorods (black curve) and the α-Fe_2O_3/CdS nanocomposites (red curve); (f) EDX analysis spectrum of the α-Fe_2O_3/CdS nanocomposites.

level and also appropriate valence band level. The fast charge separation happens at the interface of the semiconductor heterostructure and the photogenerated carriers can react with H_2O or O_2 efficiently at the surfaces.[14] α-Fe_2O_3 is one of the semiconductors which are suitable to be coupled with CdS. For example, Wang et al.[12] synthesized CdS nanowires decorated with α-Fe_2O_3 nanoparticles and found that the hybrid heterostructures showed enhanced photocatalytic activity. Also, Kundu et al.[24] used a wet chemical route to obtain heterostructures of ZnO nanorods/CdS nanoparticles that exhibited a high activity for degradation of methylene blue under solar irradiation.

In this paper, we used preformed single-crystal α-Fe_2O_3 nanorods as 1D nanoscale template for the overgrowth of CdS nanoparticles via a simple solution method with low temperature and mild reaction conditions. During the synthetic process, no surface treatments were needed to introduce any surface functional groups or linkers. The obtained cornlike 1D nanostructures of α-Fe_2O_3 nanorods/CdS nanoparticles were characterized by X-ray diffraction (XRD), scanning electron microscopy (SEM), transmission electron microscopy (TEM), high-resolution transmission electron microscopy (HRTEM), Raman spectroscopy, energy-dispersive X-ray spectroscopy (EDX), UV−vis absorption spectroscopy, photoluminescence spectroscopy and N_2 adsorption-desorption analysis techniques. The photocatalytic activities of the α-Fe_2O_3/CdS nanocomposites were evaluated by the photocatalytic degradation of a model pollutant, methylene blue (MB) under visible light. The heterostructures exhibited greatly enhanced photocatalytic activity than pure α-Fe_2O_3 nanorods.

EXPERIMENTAL SECTION

Synthesis of α-Fe_2O_3 Nanorods. The α-Fe_2O_3 nanorods were pre-synthesized by a hydrothermal method. All chemicals used in this study were of analytical grade. In a typical process, $FeCl_3$ (0.01 mol) was dissolved in deionized water (30 mL). The solution was then mixed with 15 mL of NaOH aqueous solution (2 M). The obtained precipitation was washed by deionized water for 8 times. After washing, the precipitation was dispersed in 50 mL of NaOH aqueous solution (2 M) under vigorous magnetic stirring for 1 h. Then the suspension was transferred into a 100 mL autoclave Teflon vessel and hydrothermally treated at 160 °C for 20 h. After that, the autoclave was cooled down to room temperature naturally. The resulting sample was washed with deionized water and ethanol and separated by centrifugation each for three times. The final product of the α-Fe_2O_3 nanorods were dried at 60 °C and heat treated at 400 °C for 3 h.

Synthesis of α-Fe_2O_3/CdS Cornlike Nanorods. In a typical synthetic process, α-Fe_2O_3 nanorods (0.02 g) were well-dispersed in deionized water (30 mL) under magnetic stirring and then $CdSO_4$ (0.1 mmol), thiourea (0.2 mmol) and ammonia (0.255 g) were added into the suspension. The resulting mixture was kept at 60 °C under vigorous magnetic stirring for 3 h. After the reaction was completed, the obtained solid sample was collected, washed with deionized water and ethanol, separated by centrifugation for three times, and then dried in a vacuum at 70 °C for 3 h.

To investigate the effect of CdS amount on photocatalytic activity, we prepared α-Fe_2O_3/CdS cornlike nanorods with different CdS amounts by adding more α-Fe_2O_3 nanorods (0.2 g and 0.1 g) while the other conditions remained the same.

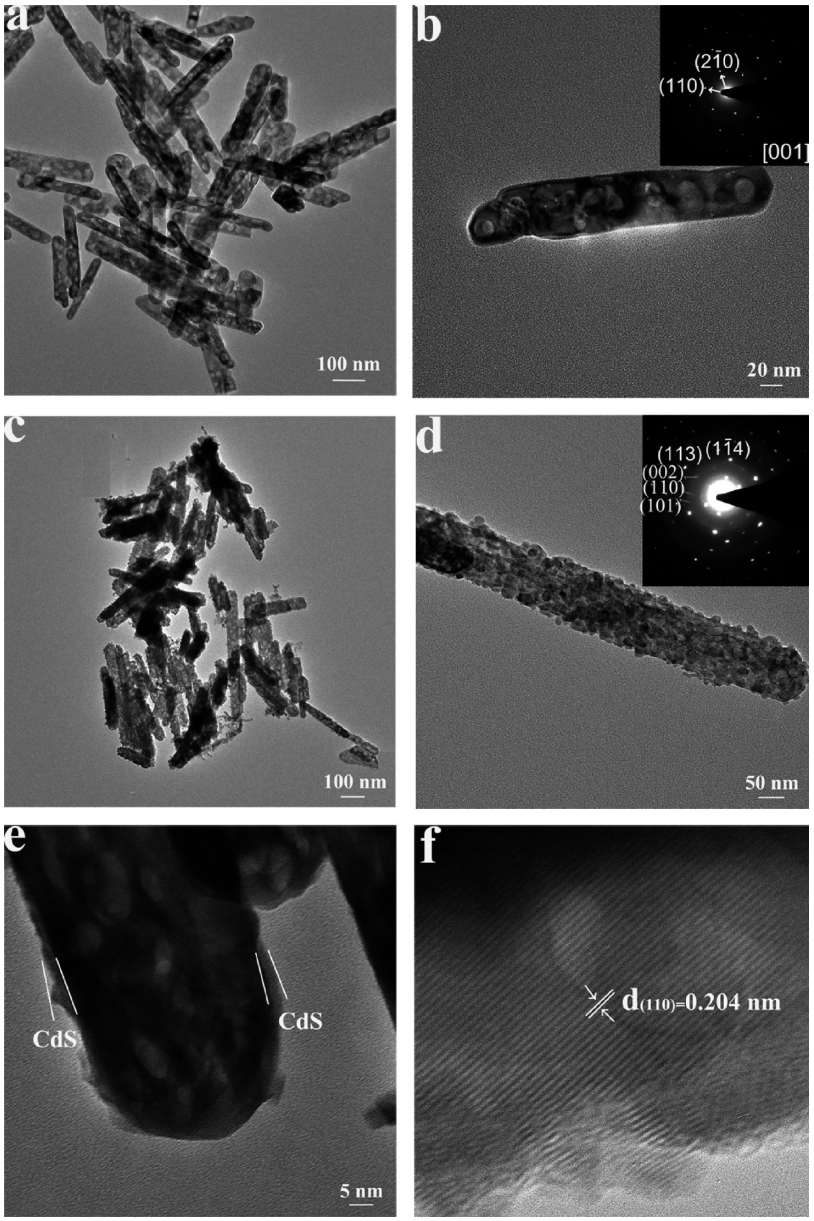

Figure 2. (a,b) TEM images of the pre-prepared α-Fe_2O_3 nanorods. Inset in b is the SAED pattern of the individual α-Fe_2O_3 nanorod. (c–e) TEM images with different magnifications and (f) HRTEM image of the α-Fe_2O_3/CdS nanocomposites. Inset in d is the SAED pattern of the single α-Fe_2O_3/CdS nanorod.

Characterization. The analysis of the crystal phases of all samples was conducted by XRD with Cu Kα radiation (RIGAKU D/MAX 2550/PC, Rigaku Corporation, Japan) at room temperature. The surface morphology of the as-prepared samples was obtained by using SEM (Hitachi S-4800, Hitachi Corporation, Japan). The samples were dropped on Al substrates and dried before the analysis. The elementary analysis was conducted by using the EDX attached to the S-4800 SEM (Hitachi S-4800 EDX, Hitachi Corporation, Japan). The microstructure of the products was investigated by TEM and HRTEM (Philips CM200, Philips Corporation, America) with an accelerating voltage of 160 kV. The selected area electron diffraction patterns (SAED) of the samples were recorded on an electron microscope (Philips CM200, Philips Corporation, America) operated at 160 kV. Nitrogen adsorption/desorption measurements were conducted at 77.35 K on a Tristar II 3020 analyzer (OMNI-SORP100CX, BECKMAN COULTER, America). The Brunauer–Emmett–Teller (BET) surface area was estimated from the adsorption data. Raman spectra of the products were recorded using a Raman spectrometer (Renishaw InVia, England). The obtained products were dispersed in ethanol for measurement of UV–vis absorption spectra on a Scan UV–vis spectrophotometer (UV-2450, Shimadzu Corporation, Japan) at room temperature from 300 to 800 nm.

Photocatalytic Activity Measurement. In this study, we used the photocatalytic degradation of MB under visible light to evaluate the photocatalytic activity of the α-Fe_2O_3/CdS cornlike nanorods, as MB is a typical model pollutant. A 300 W tungsten halide lamp was used as a light source and kept 20 cm away from the photocatalytic reactor during the photocatalytic activity measurement. In a typical run of measurement, as-obtained catalyst (5 mg) was added into 50 mL of MB solution (10 mg L^{-1}). Then the suspension was stirred for 15 min and ultrasonicated for another 15 min to reach the adsorption-desorption equilibrium between the MB and the photocatalyst in dark. After that, the suspension was continuously stirred and exposed to light irradiation while the temperature of the suspension was kept at 20 °C. Analytical samples were taken from the suspension every 0.5 h and the photocatalyst powders were separated by centrifugation. The MB concentrations of the samples were measured by the scan UV-vis spectrophotometer and monitored by checking the absorbance at 664

nm. The CdS nanoparticles used in the control experiments were synthesized by the similar method to the synthesis of α-Fe_2O_3/CdS cornlike nanorods but without the addition of α-Fe_2O_3. The size of CdS nanoparticles was similar to that of CdS particles on the α-Fe_2O_3 nanorods. Also, commercial TiO_2 (P25) was used in the control experiment.

RESULTS AND DISCUSSION

Morphology and Structure. We present the cornlike morphology and crystal structure of the nanocomposites in Figure 1. Firstly, the phase and crystalline composition of the as-prepared samples were investigated by XRD. Figure 1e shows the XRD patterns of the pre-synthesized Fe_2O_3 nanorod precursors (black curve) and the final products of Fe_2O_3/CdS composites (red curve). All the peaks of the black curve can be indexed as the hexagonal structure of α-Fe_2O_3 (JPCDS number 01-089-0597) and no other crystalline impurities are detected. The strong and sharp peaks prove that the α-Fe_2O_3 nanorods are well-crystallized. As for the composites, the peaks marked by black squares also match well with the standard XRD patterns of hexagonal hematite α-Fe_2O_3 and the other peaks marked by red circles can be indexed as hexagonal greenockite CdS (JPCDS number 00-041-1049). Compared to α-Fe_2O_3 nanorods, the peaks associated with CdS are much broader, indicative of much smaller crystalline sizes.[23] All the results demonstrate that the final product is a mixture of α-Fe_2O_3 and CdS.

The morphologies of the pre-prepared α-Fe_2O_3 nanorods and the α-Fe_2O_3/CdS nanocomposites were investigated by SEM. Images a and b in Figure 1 show the morphology of the α-Fe_2O_3 nanorods. They are 50−400 nm in width and 1−5 μm in length, with smooth surfaces. In contrast to the common α-Fe_2O_3 nanorods with shuttlelike morphology,[20,23,25] the α-Fe_2O_3 nanorods we obtained are uniform in width. Images c and d in Figure 1 are SEM images of the final products of the α-Fe_2O_3/CdS nanocomposites. Most of the α-Fe_2O_3 nanorods are coated with a layer of the CdS nanoparticles with radius of about 20 nm, thus exhibiting a cornlike morphology. With the CdS nanoparticles attached, the α-Fe_2O_3/CdS nanocomposites are up to 500 nm in width, whereas their lengths are little changed. The composition of the nanocomposites were further confirmed by EDX analysis demonstrating that the nanocomposites are composed of O, S, Cd and Fe elements (Al signal is from the Al substrates) with the molar ratio (Fe_2O_3 to CdS) of about 12:7 (Figure 1f).

The microstructure and morphology of the samples were further investigated by TEM (Figure 2). We observe a porous internal structure with spherical holes inside the pre-prepared α-Fe_2O_3 nanorods (Figure 2a, b), although the nanorods have smooth surfaces. The SAED (selected area electron diffraction) pattern of an individual α-Fe_2O_3 nanorod reconfirms the hexagonal hematite structure and shows that the nanorods are single-crystals growing along the (110) direction. The morphology of the α-Fe_2O_3/CdS nanocomposites shown in TEM images is well consistent with that in the SEM images (Figure 2c, d). It is observed that nanoparticles adhered on the surfaces of nanorods, resulting in the cornlike morphology of the nanocomposites. A further magnified TEM image (Figure 2e) reveals that part of the surface of α-Fe_2O_3 nanorods is covered by a thin layer of CdS other than CdS nanoparticles. The inset in Figure 2d presents the SAED pattern of an individual α-Fe_2O_3/CdS nanorod showing spots associated with both the α-Fe_2O_3 single crystal and the CdS nanoparticles. The clear lattice fringe can be observed in the HRTEM image (Figure 2f) and the measured lattice spacing is 0.204 nm, which is consistent with the spacing of the CdS (110) plane. Therefore, TEM, HRTEM, and SAED studies further confirm the existence of crystalline CdS on the α-Fe_2O_3 nanorods, with a unique cornlike structure. The crystalline nature of both CdS and α-Fe_2O_3 promises favored charge transportation and high photocatalytic performance.

We also used the Raman spectra to study the crystal phase and the microstructure of the α-Fe_2O_3/CdS nanocomposites. As shown in Figure 3, in the Raman spectrum of as-prepared α-

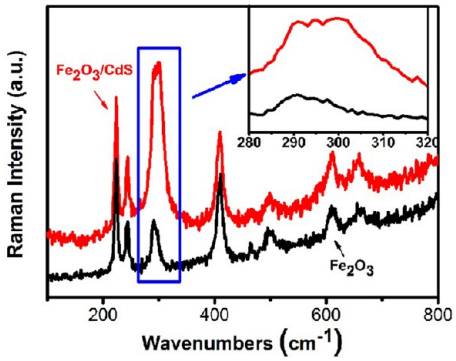

Figure 3. Raman spectra of the α-Fe_2O_3 nanorods and cornlike α-Fe_2O_3/CdS nanocomposites.

Fe_2O_3 nanorods, the peaks at 224, 245, 290, 297, 408, 496, 610, and 660 cm^{-1} can be identified as the $A_{1g}(1)$, $E_g(1)$, $E_g(2)$, $E_g(3)$, $E_g(4)$, $A_{1g}(2)$, $E_g(5)$ and E_u bands of hematite.[26] In contrast, the Raman spectrum of as-prepared Fe_2O_3/CdS composites show an additional peak at 301 cm^{-1} which can be ascribed to CdS. The intensity of this peak is significantly high and the peak is broad due to the LO (longitudinal optical) type confined vibrations of CdS nanoparticles.[27]

In order to understand the formation mechanism of α-Fe_2O_3/CdS nanocomposites, the nanocomposites with varied reaction time were examined. Figure 4 shows the SEM images of α-Fe_2O_3/CdS nanocomposites that reacted for 0.25, 1, 2, and 3 h, respectively. After 0.25 h of reaction, small particles nucleated on the surface of parts of the α-Fe_2O_3 nanorods (Figure 4a). Subsequently, more nuclei formed and covered

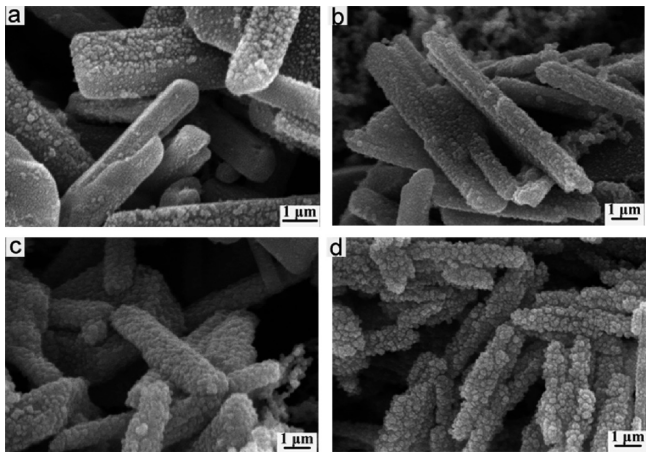

Figure 4. SEM images of α-Fe_2O_3/CdS nanocomposites with different reaction times: (a) 0.25, (b) 1, (c) 2h, and (d) 3 h.

dx.doi.org/10.1021/am3011516 | ACS Appl. Mater. Interfaces 2012, 4, 4800−4806

most of the surfaces of the nanorods (Figure 4b, c). The high density of nuclei formed is due to the high initial concentrations of CdS precursors and the relatively low nucleation barrier for the heterogeneous nucleation.[12,28] Finally, the nuclei continued to overgrow on the nanorods and the surfaces of the nanorods became rougher, exhibiting a cornlike morphology (Figure 4d).

Photocatalytic Properties. After examining the structure of the nanocomposites, we proceeded to evaluate their photocatalytic properties under visible light irradiation, using MB as the model contaminant. For comparison, the photocatalytic properties of the pre-prepared α-Fe_2O_3 nanorods and the CdS nanoparticles with similar sizes were also investigated. The characteristic absorption of MB at 664 nm was used to monitor the concentration of MB during the degradation process.[12] Figure 5a shows the evolution of the absorption

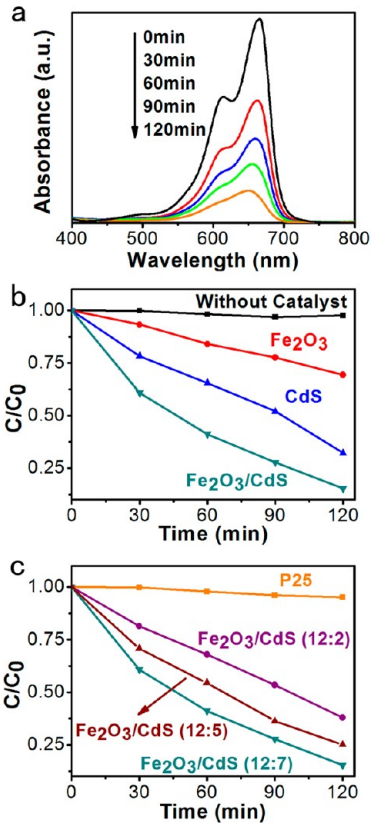

Figure 5. (a) Absorption spectra of the solution of MB exposed to irradiation for different time in the presence of α-Fe_2O_3/CdS nanocomposites as photocatalyst. (b) Photocatalytic performances of different samples under visible light irradiation: without catalyst, the pre-prepared α-Fe_2O_3 nanorods, CdS nanoparticles and the typical cornlike α-Fe_2O_3/CdS nanocomposites. (c) Photocatalytic performances of different samples under visible light irradiation: P25 and α-Fe_2O_3/CdS composites with increasing amounts of CdS.

spectra of the MB solution containing the α-Fe_2O_3/CdS nanocomposites during the photocatalytic degradation process. The absorption peak at 664 nm decreased rapidly as the irradiation time increased, indicative of the degradation of MB. After 120 min, up to 86.7% of MB was degraded in the presence of α-Fe_2O_3/CdS nanocomposites, showing a superior photocatalytic performance than the α-Fe_2O_3 nanorods and CdS nanoparticles by which only 30.6 and 63.9% of MB were degraded after the same period of time (Figure 5b). The photocatalytic activity of our α-Fe_2O_3/CdS nanocomposites is higher than that of the α-Fe_2O_3 hierarchically microspheres which manifest the best photocatalytic performances among pure α-Fe_2O_3 nanomaterials,[19] and is comparable to the best reported visible-light-driven Fe_2O_3 based photocatalyst, α-Fe_2O_3/SnO_2, while showing the advantages of low cost and facile synthesis over α-Fe_2O_3/SnO_2 nanocomposites.[29] We also compared the performance of α-Fe_2O_3/CdS nanocomposites to the widely used photocatalyst, TiO_2 (P25). The results show that α-Fe_2O_3/CdS nanocomposites exhibit higher photocatalytic activity than P25 in visible light range (Figure 5c) and their performance under visible light is comparable to that of P25 under UV irradiation.[30]

The effect of CdS amount on photocatalytic activity of α-Fe_2O_3/CdS nanocomposites was investigated. Figure 5c shows the photocatalytic performance of α-Fe_2O_3/CdS composites with different amounts of CdS. It is found that as the amount of CdS increased, the photocatalytic activity of nanocomposites increased and all the composites show higher photocatalytic activity than pure α-Fe_2O_3 nanorods. We attribute the superior performance to the following three mechanisms.

First, the α-Fe_2O_3/CdS nanocomposites show larger surface areas than the α-Fe_2O_3 nanorods. The BET (Brunauer-Emmett-Teller) surface areas of the α-Fe_2O_3 nanorods and α-Fe_2O_3/CdS nanocomposites were calculated from the nitrogen adsorption/desorption isotherms (Figure 6). The α-Fe_2O_3

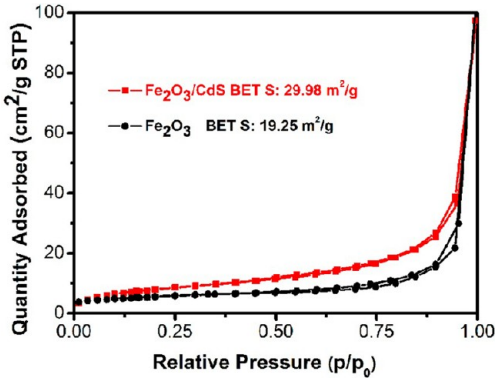

Figure 6. Nitrogen adsorption−desorption measurements and the estimated BET surface areas of the α-Fe_2O_3 nanorods and cornlike α-Fe_2O_3/CdS nanocomposites.

nanorods show a surface area of 19.25 m^2 g^{-1}, whereas the over-growth of CdS nanoparticles on the α-Fe_2O_3 nanorods greatly enhances the surface area of nanocomposites up to 29.98 m^2 g^{-1}, which is 50% higher than that of α-Fe_2O_3 nanorods. The larger surface area resulted from the rough surface of the composites can provide more reaction sites for the photocatalytic degradation of MB.[24,31,32]

Second, the α-Fe_2O_3/CdS nanocomposites show more intense absorption at the wavelength shorter than 500 nm. As important properties for photocatalysts, the UV−vis absorption spectra of the α-Fe_2O_3 nanorods and α-Fe_2O_3/CdS nanocomposites dispersed in deionized water are presented in Figure 7 (the spectra are normalized by the concentrations of the nanomaterials). It is observed that both the samples respond to the visible light, but when the wavelength is shorter than 500 nm, the absorption of the α-Fe_2O_3 nanorods fades rapidly, whereas the α-Fe_2O_3/CdS nanocomposites show much higher absorption than the pure α-Fe_2O_3. Therefore, the

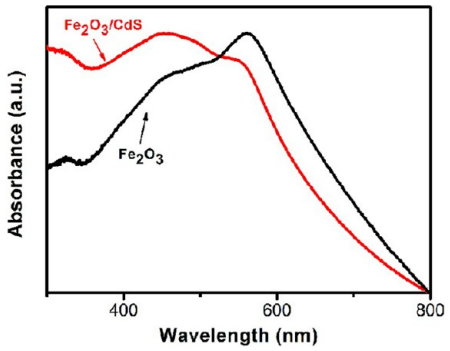

Figure 7. UV–vis absorption spectra of the α-Fe_2O_3 nanorods and cornlike α-Fe_2O_3/CdS nanocomposites.

composites absorb the light more effectively in the near-UV region, resulting in higher photocatalytic activities.

At last, the fast charge separation at the interface of the α-Fe_2O_3/CdS heterostructure due to the proper conduction bands (CB) and valence band (VB) alignment between α-Fe_2O_3 and CdS is another factor to enhance the photocatalytic activity.[14,23,33−35] The energy levels of α-Fe_2O_3 and CdS are shown in Figure 9.[12] The crystalline nature of both α-Fe_2O_3 nanorods and CdS nanoparticles further favors the fast charge separation and transport. This could be demonstrated by the photoluminescence (PL) spectra of the CdS nanoparticles and α-Fe_2O_3/CdS nanocomposites, as shown in Figure 8. We can

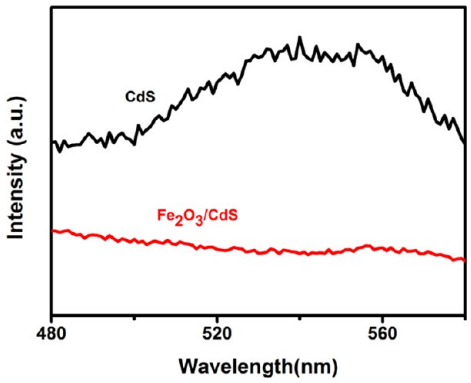

Figure 8. PL spectra of the CdS nanoparticles and cornlike α-Fe_2O_3/CdS nanocomposites.

see that after the CdS nanoparticles being combined to α-Fe_2O_3 nanorods, the PL intensity of the composites decreased rapidly, demonstrating the efficient charge separation of the composites.[36] As shown in Figure 9, once the electrons in the VB of α-Fe_2O_3 and CdS are excited to the CB under irradiation, the photo-induced electrons on the CB of CdS will transfer to the CB of α-Fe_2O_3 while the photogenerated holes on the VB of α-Fe_2O_3 will transfer to the VB of CdS. Therefore, the photogenerated electron-hole pairs could be separated more efficiently at the interface of the heterostructure and their recombination decreases. Subsequently, the photogenerated electrons and holes could migrate more effectively to the surfaces of α-Fe_2O_3 and CdS and produce the hydroxyl radicals which could decompose the MB as a powerful oxidant.[23,31]

CONCLUSION

In summary, we successfully synthesized the α-Fe_2O_3/CdS cornlike nanorods by a simple and mild two-step method. The

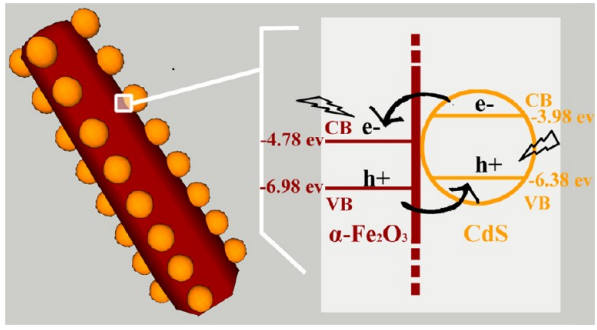

Figure 9. Schematic illustration of the charge separation at interface of the cornlike α-Fe_2O_3/CdS nanocomposites under visible light. The data are from ref 12.

microstructure of the composites was investigated, showing that crystallized CdS nanoparticles grew on the single-crystal α-Fe_2O_3 nanorods and formed the heterostructure between α-Fe_2O_3 and CdS. The photocatalytic tests proved that the α-Fe_2O_3/CdS nanocomposites exhibited excellent photocatalytic properties under visible light irradiation which could be attributed to the synergy between α-Fe_2O_3 and CdS and the cornlike nanorods structure. These results show that the α-Fe_2O_3/CdS cornlike nanorods are promising to be used as high-performance visible-light-driven photocatalyst. Our method of coupling two visible-light-response semiconductors might be used as a facile strategy for the design of high-performance photocatalyst.

AUTHOR INFORMATION

Corresponding Author

*Tel: +86-571-87952557. E-mail: hanying_li@zju.edu.cn (H.L.); hzchen@zju.edu.cn (H.C.).

Author Contributions

The manuscript was written through contributions of all authors. All authors have given approval to the final version of the manuscript.

Notes

The authors declare no competing financial interest.

ACKNOWLEDGMENTS

The authors thank the National Natural Science Foundation of China (Grants 50990063 and 51011130028) for financial support. The work was also partly supported by Fundamental Research Funds for the Central Universities (2012QNA4025).

REFERENCES

(1) Joo, J.; Kwon, S. G.; Yu, T.; Cho, M.; Lee, J.; Yoon, J.; Hyeon, T. *J. Phys. Chem. B* **2005**, *109*, 15297−15302.
(2) Xiong, Y. J.; Cai, H.; Wiley, B. J.; Wang, J.; Kim, M.; Xia, Y. N. *J. Am. Chem. Soc.* **2007**, *127*, 3665−3675.
(3) Gao, G.; Gao, W.; Guo, X.; Wang, H.; Wu, H.; Zhang, C.; Wang, C.; Cui, D. *CrystEngComm.* **2011**, *13*, 6045−6049.
(4) Liu, Z.; Zhang, D.; Han, S.; Li, C.; Lei, B.; Lu, W.; Fang, J.; Zhou, C. *J. Am. Chem.Soc.* **2004**, *127*, 6−7.
(5) Tan, L. K.; Liu, X.; Gao, H. *J. Mater. Chem.* **2011**, *21*, 11084−11087.
(6) Zhang, T. J.; Ma, Y. R.; Chen, K.; Kunz, M.; Tamura, N.; Qiang, M.; Xu, J.; Qi, L. M . *Angew. Chem., Int. Ed.* **2011**, *50*, 10361−10365.
(7) Zhang, Y.; Xu, J. Q.; Xu, P. C.; Zhu, Y. H.; Chen, X. D.; Yu, W. J. *Nanotechnology* **2010**, *21*, 285501−285508.

(8) Wu, N.; Wang, J.; Tafen, D. N.; Wang, H.; Zheng, J. G.; Lewis, J. P.; Liu, C.; Leonard, S. S.; Manivannan, A. *J. Am. Chem. Soc.* **2010**, *132*, 6679−6685.
(9) Hao, Q.; Liu, S.; Yin, X.; Wang, Y.; Li, Q.; Wang, T2010 *Solid State Sci.* **2010**, *12*, 2125-2129.
(10) Huang, Z.; Zhang, Y.; Tang, F. *Chem. Commun.* **2005**, *3*, 342−344.
(11) Peng, L.; Xie, T.; Lu, Y.; Fan, H.; Wang, D. *Phys. Chem. Chem. Phys.* **2010**, *12*, 8033−8041.
(12) Wang, L.; Wei, H.; Fan, Y.; Gu, X.; Zhan, J. *J. Phys. Chem. C* **2009**, *113*, 14119−14125. Li, Q.; Guo, B. D.; Yu, J. G.; Ran, J. R.; Zhang, B. H.; Yan, H. J.; Gong, J. R. *J. Am. Chem. Soc.* **2011**, *133*, 10878−10884.
(13) Lee, J.; Lee, Y.; Youn, J. K.; Na, H. B.; Yu, T.; Kim, H.; Lee, S. M.; Koo, Y. M.; Kwak, J. H.; Park, H. G.; Chang, H. N.; Hwang, M.; Park, J. G.; Kim, J.; Hyeon, T. *Small* **2008**, *4*, 143−152.
(14) Daskalaki, V. M.; Antoniadou, M.; Puma, G. L.; Kondarides, D. I.; Lianos, P. *Environ. Sci. Technol.* **2010**, *44*, 7200−7205. Nan, Y. X.; Chen, F.; Yang, L. G.; Chen, H. Z. *J. Phys. Chem. C* **2010**, *114*, 11911−11917. Kumar, A.; Singhal, A. *J. Mater. Chem.* **2011**, *21*, 481−496. Chen, F.; Zhou, R.; Yang, L.; Liu, N.; Wang, M.; Chen, H. Z. *J. Phys. Chem. C* **2008**, *112*, 1001−1007.
(15) Machala, L.; Tucek, J.; Zboril, R. *Chem. Mater.* **2011**, *23*, 3255−3272.
(16) Li, L.; Chu, Y.; Liu, Y.; Dong, L. *J. Phys. Chem. C* **2007**, *111*, 2123−2127. Zhou, X. M.; Lan, J. Y.; Liu, G.; Deng, K.; Yang, Y. L.; Nie, G. J.; Yu, J. G.; Zhi, L. J. *Angew. Chem., Int. Ed.* **2012**, *51*, 178−182.
(17) Katsuki, H.; Komarneni, S. *J. Am. Ceram. Soc.* **2003**, *86*, 183−185.
(18) Wang, B.; Wu, H. B.; Yu, L.; Xu, R.; Lim, T.; Lou, X. W. *Adv. Mater.* **2012**, *24*, 1111−1116.
(19) Xu, J. S.; Zhu, Y. J. *CrystEngComm.* **2011**, *13*, 5162−5169.
(20) Wang, Y.; Cao, J.; Wang, S.; Guo, X.; Zhang, J.; Xia, H.; Zhang, S.; Wu, S. *J. Phys.Chem. C* **2008**, *112*, 17804−17808. Zhu, C. L.; Yu, H. L.; Zhang, Y.; Wang, T. S.; Ouyang, Q. Y.; Qi, L. H.; Chen, Y. J.; Xue, X. Y. *ACS Appl. Mater. Interfaces* **2012**, *4*, 665−671.
(21) Yuan, S.; Zhou, Z.; Li, G. *CrystEngComm* **2011**, *13*, 4709−4713.
(22) Chen, J. S.; Zhu, T.; Yang, X. H.; Yang, H. G.; Lou, X. W. *J. Am. Chem. Soc.* **2010**, *132*, 13162−13164.
(23) Zhu, L. P.; Bing, N. C.; Yang, D. D.; Yang, Y.; Liao, G. H.; Wang, L. J. *CrystEngComm* **2011**, *13*, 4486−4490.
(24) Kundu, P.; Deshpande, P. A.; Madras, G.; Ravishankar, N. *J. Mater. Chem.* **2011**, *21*, 4209−4216.
(25) Wu, W.; Zhang, S. F.; Xiao, X. H.; Zhou, J.; Ren, F.; Sun, L. L.; Jiang, C. Z. *ACS Appl. Mater. Interfaces* **2012**, DOI: 10.1021/am300669a. Pradhan, G. K.; Parida, K. M. *ACS Appl. Mater. Interfaces* **2011**, *3*, 317−323.
(26) Olga, P. L.; Shebanova, N. *J. Raman Spectrosc.* **2003**, *34*, 845−853.
(27) Rajeev, M. A. K.; Prabhu, R. *Bull. Mater. Sci.* **2008**, *31*, 511−516.
(28) Zhou, W.; Liu, X.; Cui, J.; Liu, D.; Li, J.; Jiang, H.; Wang, J.; Liu, H. *CrystEngComm* **2011**, *13*, 4557−4563.
(29) Kang, J.; Kuang, Q.; Xie, Z. X.; Zheng, L. S. *J. Phys. Chem. C* **2011**, *115*, 7874−7879.
(30) Pan, J. H.; Cai, Z. Y.; Yu, Y.; Zhao, X. X. *J. Mater. Chem.* **2011**, *21*, 11430−11438.
(31) Zhao, X. W.; Jin, W. Z.; Cai, J. G.; Ye, J. F.; Li, Z. H.; Ma, Y. R.; Xie, J. L.; Qi, L. M. *Adv. Funct. Mater.* **2011**, *21*, 3554−3563.
(32) Yu, X.; Liu, S.; Yu, J. *Appl. Catal. B: Environ.* **2011**, *104*, 12−20.
(33) Zhang, J.; Liu, X. H.; Wang, L. W.; Yang, T. L.; Guo, X. Z.; Wu, S. H.; Wang, S. R.; Zhang, S. M. *Nanotechnology* **2011**, *22*, 185501−185508.
(34) Xiong, Y. J.; Wiley, B. J.; Xia, Y. N. *Angew. Chem. Int. Ed.* **2007**, *46*, 7157−7159.
(35) Dong, Y. J.; Yu, G. H.; McAlpine, M. C.; Lu, W.; Lieber, C. M. *Nano Lett.* **2008**, *8*, 386−391.
(36) Liu, Y.; Yu, L.; Hu, Y.; Guo, C. F.; Zhang, F. M.; Lou, X. W. *Nanoscale* **2012**, *4*, 183−187.